



## Establishment of a 3D multi-layered *in vitro* model of inflammatory bowel disease

Bárbara Ferreira<sup>a,b,c</sup>, Cecília Ferreira<sup>a,b,c,d</sup>, Cláudia Martins<sup>a,b</sup>, Rute Nunes<sup>a,b,e</sup>,  
José das Neves<sup>a,b,e</sup>, Catarina Leite-Pereira<sup>a,b</sup>, Bruno Sarmento<sup>a,b,e,\*</sup>

<sup>a</sup> i3S – Instituto de Investigação e Inovação em Saúde, Universidade do Porto, Rua Alfredo Allen 208, 4200-135 Porto, Portugal

<sup>b</sup> INEB – Instituto de Engenharia Biomédica, Universidade do Porto, Rua Alfredo Allen 208, 4200-135 Porto, Portugal

<sup>c</sup> ICBAS – Instituto de Ciências Biomédicas Abel Salazar, Universidade do Porto, Rua de Jorge Viterbo Ferreira 228, 4050-313 Porto, Portugal

<sup>d</sup> FCUP – Faculdade de Ciências da Universidade do Porto, Universidade do Porto, Porto, Portugal

<sup>e</sup> IUCS-CESPU – Instituto Universitário de Ciências da Saúde, Rua Central de Gandra 1317, 4585-116 Gandra, Portugal

### ARTICLE INFO

#### Keywords:

Inflammatory bowel disease  
D intestinal model  
Immune system  
Collagen-alginate matrix  
Tissue engineering

### ABSTRACT

Crohn's Disease and Ulcerative Colitis, the main types of Inflammatory Bowel Disease (IBD), are life-threatening gastrointestinal disorders with no definitive cure. The establishment of biorelevant *in vitro* models that closely recapitulate the IBD microenvironment is of utmost importance to validate newly developed IBD therapies. To address the existing flaws in the current representation of the IBD microenvironment, we propose a novel three-dimensional (3D) *in vitro* model comprising a multi-layered gastrointestinal tissue with functional immune responses under inflammatory conditions. The multi-layered architecture consists of a lamina propria-like hydrogel with human intestinal fibroblasts (HIF), supporting an epithelial layer composed of Caco-2 and HT29-MTX cells, along with an endothelial layer surrogating the absorptive capillary network. A collagen-alginate composite matrix was optimized for the lamina propria-like hydrogel, preserving HIF metabolic activity and morphology over time. To achieve immune competence, pre-differentiated THP-1-derived macrophages were incorporated into the epithelial barrier. Inflammation was induced through the optimization of an inflammatory cocktail consisting of *E. coli* O111:B4 lipopolysaccharide combined with a specialized cytokine array (tumor necrosis factor- $\alpha$ , interferon- $\gamma$ , and interleukin-1 $\beta$ ). This inflammation-inducing stimulus led to a significant upregulation of pro-inflammatory cytokines commonly associated with IBD onset, including CCL20, IL-6, CXCL9 and CXCL10. Altogether, this 3D *in vitro* model has the potential to accelerate the drug development pipeline by providing reliable permeability and efficacy outputs for emerging therapies, reducing unnecessary animal experiments. Moreover, it offers a valuable *in vitro* platform for studying IBD pathophysiology and cell interplay dynamics.

### 1. Introduction

Inflammatory Bowel Disease (IBD) represents a group of relapsing-remitting gastrointestinal disorders, with Crohn's Disease (CD) and Ulcerative Colitis (UC) being the most prominent types [1]. IBD is highly debilitating, and a definitive cure remains elusive [2]. In North America and Europe, over 1.5 and 2 million people suffer from these diseases, respectively [3]. Genetic susceptibility, environmental factors, microbial factors, dysbiosis, intestinal barrier damage, and immune dysregulation contribute to the pathogenesis of IBD [4]. Although the precise cause of IBD remains unspecified, the most widely accepted hypothesis

to date suggests that IBD results from the hyperactivation of the intestinal immune system against the gut microbiota, triggered by environmental factors in a genetically susceptible host [1,5]. Several mechanisms are disrupted in the IBD mucosa, including the loss of barrier-forming tight junctions (TJs) and heterogeneity in the thickness and composition of the protective mucus layer. Together, these mechanisms enable the translocation of gut microbiota into the intestinal wall leading to the activation of the immune system [6]. Abnormal goblet cell function and dysfunctional Paneth cell mechanisms have also been observed in IBD [7]. From an immunological perspective, the dynamics of immune cell interactions are crucial in the inflammatory response.

\* Corresponding author at: Nanomedicines & Translational Drug Delivery Group Leader, i3S - Instituto de Investigação e Inovação em Saúde, Rua Alfredo Allen, 208, 4200-135 Porto, Portugal.

E-mail address: [bruno.sarmento@i3s.up.pt](mailto:bruno.sarmento@i3s.up.pt) (B. Sarmento).

<https://doi.org/10.1016/j.jconrel.2024.11.070>

Received 1 October 2024; Received in revised form 5 November 2024; Accepted 26 November 2024

Available online 30 November 2024

0168-3659/© 2024 The Authors. Published by Elsevier B.V. This is an open access article under the CC BY-NC license (<http://creativecommons.org/licenses/by-nc/4.0/>).

Dendritic cells, macrophages, and innate lymphocytes release pro-inflammatory cytokines that recruit additional immune cells to the site of inflammation [8]. Macrophages, in particular, act as the first line of defense in the intestinal mucosa. They not only initiate and perpetuate the inflammatory response but also contribute to its resolution. Despite their essential roles, the balance between pro-inflammatory and anti-inflammatory cytokines is often disrupted in IBD, leading to persistent and chronic inflammation [9]. A major driver of this dysregulation is the upregulation of pattern recognition receptors (PRRs) such as Toll-like receptors (TLR2 and TLR4), CD40, and the chemokine receptor 7 (CCR7) on dendritic cells and macrophages [10,11]. These receptors initiate inflammatory responses by triggering the release of pro-inflammatory cytokines, including tumor necrosis factor- $\alpha$  (TNF- $\alpha$ ), interleukin-1 $\beta$  (IL-1 $\beta$ ), and IL-6. For instance, TNF- $\alpha$  and interferon- $\gamma$  (IFN- $\gamma$ ) contribute to increased epithelial paracellular permeability by disrupting TJ integrity [12]. This disruption facilitates the translocation of luminal antigens, thereby perpetuating the inflammatory response, and promoting further tissue damage. IL-6 enhances immune cell recruitment and activation, which increases the production of additional inflammatory mediators [13]. Specifically, IL-8, a potent chemoattractant for neutrophils, amplifies the inflammatory response within the intestinal mucosa. In contrast, anti-inflammatory cytokines such as IL-10 help counterbalance this response by inhibiting pro-inflammatory pathways, promoting epithelial repair, and restoring TJ integrity [14]. C-X-C motif chemokine 10 (CXCL10), a chemokine upregulated in response to inflammatory stimuli, is crucial for monocyte activation by IFN- $\gamma$ , leading to increased production of pro-inflammatory cytokines like IL-12 and IL-23. Moreover, elevated levels of chemokine (C–C motif) ligand 20 (CCL20) in the colonic mucosa of IBD patients exacerbate intestinal inflammation by recruiting both regulatory T cells and T helper 17 cells [15]. Furthermore, the balance between effector and regulatory T cells appears disturbed in the IBD mucosa, leading to uncontrolled activation of different T-cell lineages [7].

*In vitro* models have been crucial in studying the pathophysiology of IBD and in advancing the development of novel therapeutic approaches [16–18]. However, traditional two-dimensional (2D) cell culture models fail to accurately reproduce the *in vivo* conditions of cell growth, spreading, migration, and tissue architecture [19]. The Caco-2 cell line, derived from human colon adenocarcinoma, remains the gold standard for *in vitro* intestinal permeability assays [20]. More evolved models have used co-culture models in Transwell® inserts where intestinal epithelial cells and immune cells are cultured separately, limiting direct cell-cell interactions. Some studies have innovated by including both cell types in the same compartment [21] or by using inverted models [22–29]. Despite these advancements, 2D co-culture systems still struggle to replicate the complex three-dimensional (3D) architecture and dynamic microenvironment of the intestinal tissue *in vivo*, leading to a limited representation of cell-cell and cell-matrix interactions [30]. In response to these limitations, 3D culture models have emerged as a promising alternative. The models not only provide 3D architecture for cell growth but also facilitate cell-cell and cell-extracellular matrix (ECM) interactions [31,32]. One important contribution in accurately mimicking cellular behavior in 3D cultures is the use of matrices and scaffolds, which are typically composed of ECM components. Collagen is particularly favored for its affordability, ease of processing, and flexibility for live-cell manipulation. Its properties, such as stiffness, nano/micro-porosity, biodegradability, and pore interconnectivity, make it an excellent choice [33,34]. Other materials, including alginate, Matrigel®, synthetic polymers, and decellularized ECM can also be used to improve matrix mechanics and biointegration [35]. Despite significant advances in the development of 3D intestinal models, from scaffold- and hydrogel-based systems to decellularized tissues, and more complex gut-on-a-chip models and organoids, several challenges remain, highlighting the need for further innovation in this field [16,17,36–38]. Specifically, these models often fail to fully replicate the complexity of

the intestinal microenvironment and may not precisely reproduce the interface between the intestinal epithelium and the lamina propria. To address these limitations, we aim to advance the state of the art by developing an innovative 3D multi-layered model of IBD that takes into consideration the 3D intestinal architecture and the key cellular components involved in IBD pathogenesis. We have previously developed a 3D multi-layered *in vitro* intestinal model for testing drug absorption [39,40]. This model was able to mimic the intestinal lamina propria through a collagen-based stromal layer with embedded human intestinal fibroblasts (HIF), and the epithelial layer composed of Caco-2 and HT29-MTX cells. Also, to mimic the blood vessel barrier, an endothelial layer underneath the lamina propria was co-cultured. In this work, we invested further efforts to modulate the biorelevance of the previously developed 3D model for IBD by providing immune competence through the addition of immune cells, particularly macrophages, giving their key role in establishing the inflammatory environment (Fig. 1). Moreover, specialized inflammatory cocktails were designed and optimized to induce an IBD-like inflammatory microenvironment. This advanced 3D model aims to provide a novel and reproducible platform for IBD cell interplay studies and preclinical drug testing, improving our understanding of disease pathophysiology, and possible alterations in drug absorption and efficacy due to intestinal inflammation.

## 2. Methods

### 2.1. Cell culture

C2BBE1 clone of Caco-2 (regarded as Caco-2 cells in the manuscript) were purchased from American type culture collection (ATCC, USA). Cells (passage 53 to 80) were cultured with Dulbecco's Modified Eagle Medium (DMEM) supplemented with 100 U/mL of penicillin and 100  $\mu$ g/mL of streptomycin (Biowest), 10 % (v/v) Fetal Bovine Serum (FBS) (Biochrom GmbH), and 1 % (v/v) non-essential aminoacids (Thermo-Fisher Scientific).

Mucus producing HT29-MTX cells were kindly provided by Dr. T. Lesuffleur (INSERM U178, Villejuif, France). HT29-MTX cells (passage 41 to 55) were grown in DMEM supplemented with 100 U/mL of penicillin and 100  $\mu$ g/mL of streptomycin (Biowest), and 10 % (v/v) FBS (Biochrom).

Human intestinal fibroblasts (HIF) (passage 6) were obtained from ScienCell and were cultured in Fibroblast medium (FM) supplemented with 2 % (v/v) FBS, 1 % (v/v) of Fibroblast Growth Supplement (FGS), and 100 U/mL of penicillin and 100  $\mu$ g/mL of streptomycin (all from ScienCell).

Human pulmonary microvascular endothelial cells (HPMEC-ST1.6R cells) were kindly provided by Professor C. James Kirkpatrick (Institute of Pathology, Johannes Gutenberg University of Mainz, Germany). Cells were cultured (passage 39 to 45) with M-199 medium (Merck) supplemented with 20 % (v/v) FBS (Biochrom), 100 U/mL of penicillin and 100  $\mu$ g/mL of streptomycin (Biowest), 25  $\mu$ g/mL of Endothelial Cell Growth Supplement (ECGS) (Merck), 25  $\mu$ g/mL of heparin sodium salt from porcine intestinal mucosa (Merck) and 0.1 mg/mL L-glutamine (LabClinics).

THP-1 monocytes (TIB-202™) were also acquired from ATCC. Cells were cultured in T75 cell culture flasks as a suspension (passage number between 10 and 42) with RPMI-1640 medium (ATCC, USA) supplemented with 100 U/mL of penicillin and 100  $\mu$ g/mL of streptomycin (Biowest) and 10 % (v/v) FBS (Biochrom).

All cells were cultured separately in 75 cm<sup>2</sup> T-flasks and maintained in an incubator with a humidified atmosphere at 37 °C and 5 % CO<sub>2</sub>.

### 2.2. *In vitro* recreation of the lamina propria

#### 2.2.1. Collagen hydrogel with human intestinal fibroblasts embedded

To obtain the collagen hydrogel layer with HIF, 10 $\times$  Phosphate Buffered Saline (PBS) and fibroblast medium with HIF (5  $\times$  10<sup>4</sup> cells/

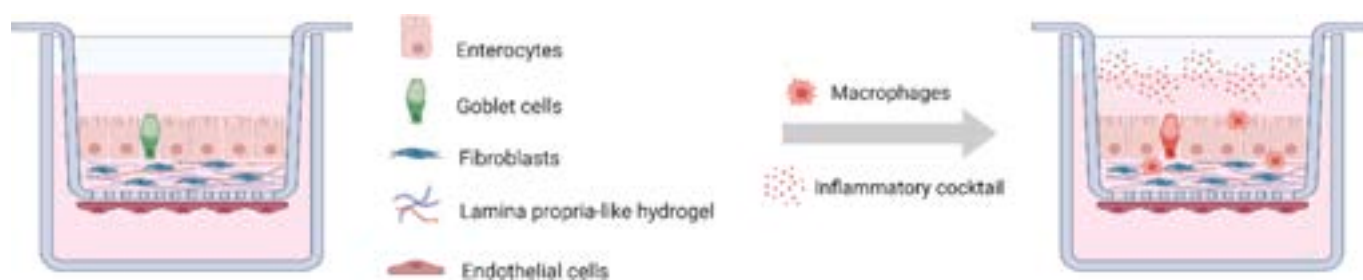


Fig. 1. Schematic representation of the 3D multi-layered model of IBD. Image created with Biorender.com

mL) were added to the high concentrated rat tail collagen type I solution (Corning), followed by titration to pH 7.4 with 1 N sodium hydroxide (NaOH) according to the supplier recommendations, to obtain the desired collagen concentration, as described in a previous study from our team [39,40]. The solution was carefully dispersed on the 12-well Transwell® inserts (Millicell) to cover the entire surface of the insert. The inserts were then incubated at 37 °C under a water-saturated atmosphere containing 5 % CO<sub>2</sub> for 30 min to allow gelation. The hydrogels were monitored for 21 days. Volumes of 0.5 mL and 1.5 mL DMEM were added to the apical and basolateral compartments of the inserts, respectively. Several strategies have been proposed to prevent collagen contraction by fibroblasts, including modulating collagen concentration, adjusting the initial seeding density of fibroblasts within the hydrogels, or incorporating alginate into the matrix [41–43]. Two collagen concentrations (6 and 7 mg/mL) were tested, along with different hydrogel volumes per insert (110, 180, and 200  $\mu$ L).

### 2.2.2. Mechanical reinforcement of collagen hydrogel with alginate

To obtain a mechanically reinforced composite hydrogel of rat tail collagen type I and alginate (collagen-alginate hydrogels), 10 $\times$  PBS and fibroblast medium with HIF were added to a high concentrated rat tail collagen solution (Corning), followed by titration to pH 7.4 with 1 N NaOH according to the supplier recommendations. Collagen and alginate solutions were mixed at a 75:25 ratio. The initial collagen solution was prepared at a concentration of 8 mg/mL, and the initial alginate solution was prepared at a concentration of 4 mg/mL. The solution was dispersed on the 12-well Transwell® inserts (Millicell) to cover the entire surface of the insert. Gel formation was achieved by an initial incubation at 37 °C to promote collagen type I polymerization followed by incubation with 100 mM CaCl<sub>2</sub> to induce alginate cross-linking. After gel formation, 0.5 mL and 1.5 mL of DMEM were added to the apical and basolateral compartments of the inserts, respectively. Here, the collagen concentration and HIF initial seeding density were maintained constant at 6 mg/mL and 5  $\times$  10<sup>4</sup> cells/mL, respectively, along with three varying alginate concentrations (2.5, 5, and 10 mg/mL). In a subsequent attempt, two alginate concentrations, 1 and 2.5 mg/mL, were tested, along with two HIF densities, 1  $\times$  10<sup>5</sup> and 2  $\times$  10<sup>5</sup> cells/mL.

### 2.2.3. Analysis of the rheological properties of collagen-alginate hydrogels

The rheological properties of the hydrogels (collagen, collagen-alginate, and collagen-alginate with cells) were assessed using a Kinexus Pro Rheometer (Malvern Instruments Ltd., UK), and all analyses were obtained using the rSpace for Kinexus software. Samples were loaded on an 8-mm parallel geometry plate with a manual gap setup. Dynamic oscillatory frequency sweep measurements were performed at 37 °C, within the linear viscoelastic region, at 1 % strain and a frequency ranging from 0.1 to 10 Hz to determine Young's modulus.

### 2.2.4. Evaluation of maintenance of metabolic activity of the human intestinal fibroblasts

The fibroblastic integrity of the hydrogels-embedded HIF was assessed by evaluating their metabolic activity (7, 14, and 21 days) using the resazurin assay, and analyzing their morphology through

fluorescence microscopy. Briefly, the resazurin solution was obtained by dissolving 50 mg of resazurin sodium salt (Sigma) into 25 mL of PBS 20 $\times$  and 475 mL of dH<sub>2</sub>O overnight, at room temperature (RT) with agitation in the dark, and then filtered. At each time point (collagen-alginate hydrogels with 7, 14, and 21 days in culture), a solution containing 20 % resazurin in DMEM complete was prepared. The solution was pre-warmed to 37 °C, and 600  $\mu$ L of solution was added to each well. The plate was incubated for 2 h at 37 °C and 5 % CO<sub>2</sub>, in a water-saturated atmosphere. After the incubation period, 3 samples of 150  $\mu$ L from each well were collected and quantified by measuring the relative fluorescence units (RFU) using a microplate reader Synergy™ Mx HM550 (Biotek) set at 530/590 nm (excitation/emission wavelength, respectively) and results were normalized by subtracting the blank (collagen hydrogel without cells).

### 2.2.5. Assessment of morphology of the human intestinal fibroblasts and secretion of extracellular matrix

For the assessment of HIF morphology and ECM secretion in the lamina propria-like matrix, after 21 days in culture, the hydrogels with HIF were washed once with Hanks' Balanced Salt Solution (HBSS) and fixed using 4 % paraformaldehyde (PFA) (Delta Microscopies) in HBSS for 30 min at RT. This step was followed by permeabilization with a solution of 0.5 % (v/v) Triton X-100 (Sigma) in HBSS for 10 min at RT and samples were washed thrice with HBSS for 5 min. After, a blocking step was performed using a blocking solution containing 2 % bovine serum albumin (BSA) (VWR) in HBSS, for 1 h at RT. Samples were then incubated with mouse anti-human vimentin (1:50) (sc-6260, Santa Cruz Biotechnology), and mouse anti-human phalloidin (1:200), at 4 °C. After incubation with the primary antibodies, samples were washed three times for 5 min with a solution of 2 % BSA (VWR) in HBSS. This was followed by incubation with the secondary antibodies: Goat anti-Rabbit IgG (H + L) Cross-Adsorbed, Alexa Fluor 488 (1:500) (A-11008, Invitrogen), and cell nuclei was counterstained with 4',6'-diamino-2-fenil-indol (DAPI) (500 ng/mL) (Merck). Finally, hydrogels were washed three times with HBSS for 5 min and kept in HBSS until visualization in Opera Phenix Plus High-Content Screening System.

## 2.3. THP-1 monocyte differentiation

### 2.3.1. Monocyte to macrophage differentiation

To induce a macrophage-like phenotype, THP-1 cells were plated in 24-well plates at a density of 2.5  $\times$  10<sup>5</sup> cells/well, with medium containing 100 ng/mL of phorbol 12-myristate 13-acetate (PMA) (Sigma). Cells were allowed to differentiate for 48 h, during which time, the THP-1 cells adhered to the surface of the wells and were thereafter referred to as "macrophages". To obtain macrophages at a resting state, adherent cells were cultured in medium without PMA for an additional 24 h [44].

### 2.3.2. Flow cytometry studies

THP-1 monocyte differentiation induced by PMA was confirmed by flow cytometry. Adherent cells were detached by adding 150  $\mu$ L of accutase for 30 min, at 37 °C. Subsequently, approximately 2.5  $\times$  10<sup>5</sup> cells/well were collected with a cell scraper into a 15 mL falcon tube and

centrifuged at 1200 rpm for 5 min, at 4 °C. Following centrifugation, the supernatant was removed, and the cells were washed with FACS buffer (700  $\mu$ L) (PBS 1 $\times$  containing 2 % FBS and 0.01 % sodium azide) and transferred to a non-coated round bottom 96-well plate (Corning Costar®). Cells were then centrifuged (1500 rpm, 5 min, 4 °C), resuspended in 50  $\mu$ L of a solution of FACS buffer with the antibodies (anti-CD86-FITC 1:25 (ImmunoTools), anti-CD163-PE 1:25 (Enzifarma) and anti-CD14-APC 1:25 (ImmunoTools)) and incubated for 30 min in the dark at 4 °C. After incubation, cells were washed twice with FACS buffer (1500 rpm, 5 min, 4 °C) and fixed in a solution of PFA 1 % (v/v). Non-stimulated THP-1 cells and unlabeled THP-1 macrophages were used as negative controls. To analyze the samples, they were filtered through a 70  $\mu$ m pore filter membrane and analyzed using the BD Accuri™ C6 flow cytometer (BD Biosciences, San Jose, United States of America). FlowJo v10 software was used to process flow cytometry data.

### 2.3.3. Transmission electron microscopy studies

THP-1 monocyte differentiation induced by PMA was further confirmed by Transmission Electron Microscopy (TEM). THP-1 cells differentiated with PMA were detached by adding 150  $\mu$ L of accutase for 30 min, at 37 °C. Subsequently, approximately  $2.5 \times 10^5$  cells/well were collected with a cell scraper into a 15 mL falcon tube and centrifuged at 1200 rpm for 5 min, at 4 °C. For the ultrastructure analysis, cells were fixed in a solution of 2.5 % glutaraldehyde with 2 % formaldehyde in 0.1 M sodium cacodylate buffer (pH 7.4) for 1 h at RT. Cells were then post-fixed in 1 % osmium tetroxide and 1.5 % potassium ferrocyanide in 0.1 M cacodylate buffer for 1 h. After centrifugation, the pellet was stained with an aqueous 1 % uranyl acetate solution overnight, dehydrated, and embedded in Embed-812 resin (#14120; Electron Microscopy Sciences). Ultra-thin sections (50 nm thickness) were cut on a RMC Ultramicrotome (PowerTome, USA) using Diatome diamond knives, mounted on mesh copper grids (Electron Microscopy Sciences), and stained with uranyl acetate substitute (#11000; Electron Microscopy Sciences) and lead citrate (#11300; Electron Microscopy Sciences) for 5 min each. Samples were viewed on a JEOL JEM 1400 transmission electron microscope (JEOL, Tokyo, Japan) and images were digitally recorded using a CCD digital camera Orius 1100 W (Tokyo, Japan).

## 2.4. Model assembly

HPMEC-ST1.6R cells were seeded at a seeding density of  $5 \times 10^4$  cells/cm<sup>2</sup> by inverting 12-well Transwell® inserts onto 6-well plates. The basolateral side of each insert was coated with 100  $\mu$ L of 0.2 % gelatin (Merck) for 1 h at RT to promote cellular adhesion. After this period, the excess gelatin was removed, and 100  $\mu$ L of HPMEC cell suspension was added. The cells were allowed to adhere for 2 h at RT, and 1 mL of PBS was added to each well to maintain humidity and prevent drying. Following adhesion, the Transwell® inserts were returned to their normal configuration in 12-well plates (VWR), and 1 mL of DMEM was added to the basolateral compartment. Following that, collagen-alginate hydrogels were prepared with 6 mg/mL collagen, 1 mg/mL alginate, and  $10^5$  HIF/mL as previously described. After a 30-min gelation process, a mixture of Caco-2 and HT29-MTX cells (9:1 ratio, respectively) was seeded on top of the fibroblast-embedded collagen-alginate layer at a seeding density of  $10^5$  cells/cm<sup>2</sup> in 0.5 mL of DMEM. Then, 1.5 mL of DMEM was added to the basolateral side, and the plates were incubated at 37 °C, with 5 % CO<sub>2</sub> in a water-saturated atmosphere. On day 19, macrophages were introduced in the 3D model. The cultures were maintained for 21 days to promote the differentiation of Caco-2 cells into enterocyte-like cells. The medium on both the apical and basolateral sides was changed every 2–3 days.

### 2.4.1. Assessment of cell layer formation, and tight junction expression

The formation of an intact layer was confirmed using an antibody against epithelial cell adhesion molecule (EpCAM) and the presence of TJs was assessed using zonula occludens-1 (ZO-1), a peripheral TJ

protein. The 3D models were washed with HBSS and fixed with 4 % PFA for 30 min. Following fixation, the 3D models were washed three times with HBSS. Permeabilization was performed using a solution of 0.5 % (v/v) Triton X-100 (Sigma) in HBSS for 10 min at RT. Afterward, the hydrogels were washed three times with HBSS for 5 min each. A blocking step was carried out using a blocking solution containing 2 % BSA in HBSS for 1 h at RT. The hydrogels were then incubated overnight at 4 °C with primary antibodies diluted in 2 % BSA in HBSS: mouse anti-human EpCAM primary antibody (1:250, Invitrogen) and rabbit anti-human ZO-1 primary antibody (1:50, sc-10,804, Santa Cruz Biotechnology). Then, the hydrogels were washed three times for 5 min each with 2 % BSA in HBSS. Next, the hydrogels were incubated with secondary antibodies and DAPI to counterstain the nuclei (500 ng/mL, Sigma). The secondary antibodies used were F(ab')<sub>2</sub>-Goat anti-Mouse IgG (H + L) Cross-Adsorbed, Alexa Fluor 594 (A-11020, Thermo Fisher Scientific) (1:500), and Goat anti-Rabbit IgG (H + L) Cross-Adsorbed, Alexa Fluor 488 (A-11008, Thermo Fisher Scientific) (1:500). Secondary antibody incubation was performed for 1 h at RT in the dark. Finally, the hydrogels were washed three times with HBSS for 5 min each and kept in HBSS until visualization using a laser scanning confocal laser scanning microscope (SP8, Leica).

## 2.5. Establishment of the inflammation model

### 2.5.1. Induction with *E. coli* O111:B4 lipopolysaccharide (LPS)

The 3D model with the endothelial layer was obtained as previously described [40] and further complemented with immune cells – macrophages ( $0.25 \times 10^6$  cells/mL). These last were obtained through the differentiation of THP-1 cells with PMA as described. To emulate the gut inflammation, 100 ng/mL LPS (Invivogen) was chosen as the pro-inflammatory inducer and added to the apical compartment of the Transwell® on day 21 for 24 h. The apical and basolateral cell culture medium was collected and analyzed to determine the levels of multiple cytokines by enzyme-linked immunosorbent assay (ELISA).

### 2.5.2. Induction with cytokine cocktails

Based on the results obtained from the LPS stimulus, specific cytokine cocktails were selected for their ability to activate diverse pathways that increase the secretion of multiple cytokines and chemokines, mirroring the inflammatory profile seen in IBD patients [45,46]. Each cytokine cocktail was added to the 3D intestinal model at concentrations of 1 ng/mL (A/B) and 10 ng/mL (A'/B'). Two different strategies were proposed for the addition of macrophages and the cytokine cocktail: (i) On day 14 of the 3D model, macrophages were added to the apical compartment of the 3D intestinal model, and the cytokine cocktail on day 19. Half of the medium was collected 24 h later (day 20) and replaced with fresh medium. On day 21, the medium was collected again for further analysis, representing 48 h post-stimulation. (ii) On day 19 of the 3D model, macrophages were added to the apical compartment of the 3D intestinal model, and the cytokine cocktail on day 20. Half of the medium was collected 24 h later (day 21) and replaced with fresh medium. The collected medium was centrifuged at 10,000  $\times$ g for 10 min and stored at –20 °C until further analysis using a multiplex assay.

### 2.5.3. Induction with a cytokine cocktail on single cells

Cocktail A was chosen for further experiments based on the preliminary results.

Caco-2, HT29-MTX, HPMEC, and HIF cells were cultured and expanded for up to 6 days. On day 6, the culture medium was collected (as a control before stimulation) and replaced with fresh medium containing cocktail A for 24 h.

For THP-1 cells, differentiation was induced using PMA, as previously described. Post-differentiation, THP-1 cells were also stimulated with cocktail A for 24 h. After the 24-h treatment period, the culture medium from all cell lines was collected and centrifuged to remove cellular debris. The supernatant was then analyzed using ELISA to

quantify specific cytokines and chemokines levels, including IL-6, IL-8, IL-12, CCL20, and CXCL10.

#### 2.5.4. Induction with the selected cytokine cocktail + LPS on the 3D model

Inflammation induction using Cocktail A and LPS (100 ng/mL) was assessed in the optimized 3D lamina propria-like model, which consists of a collagen-alginate layer (6 mg/mL collagen and 1 mg/mL alginate). Macrophages were introduced on day 19, followed by stimulation of the 3D model on day 20. After 24 h (day 21), the medium was collected for analysis. Concurrently, an experiment extended to 25 days was conducted to monitor cytokine and chemokine levels post-stimulus removal. All experiments were performed in triplicates, and the secretome was analyzed with a focus on cytokines and chemokines commonly elevated in IBD (IL-8, IL-6, CCL20, and CXCL10).

#### 2.5.5. Evaluation of the immune profile of the 3D immune-competent model

To assess the cellular response within the 3D model to each tested stimuli, the levels of cytokines and chemokines were measured either using enzyme-linked immunosorbent assay (ELISA) (Table 1), or a multiplex array, using the Bio-Plex Pro Human Chemokine Panel, 40-Plex - Bio-Rad Laboratories (reference #171AK99MR2) (Table 2).

### 2.6. Statistical analysis

Statistical analysis was performed using the GraphPad Prism 9.02 software. The experiments were performed with at least three biological repeats with three technical repeats within each biological repeat. Error bars represent  $\pm$ SD. Statistical analysis was performed using either analysis of variance (two-way ANOVA) with Kruskal-Wallis or Mann-Whitney post-hoc test and Student's *t*-test. The significance level set probabilities of  $*p < 0.05$ ,  $**p < 0.01$  and  $***p < 0.001$ .

## 3. Results and discussion

### 3.1. Optimization of the lamina propria-like matrix

To establish a 3D model of IBD, a collagen hydrogel layer with embedded HIF was optimized to mimic the intestinal lamina propria, which acts as a supporting layer for epithelial cells in the small intestine. Collagen contraction is a widely recognized challenge in hydrogel-based models, primarily caused by the contractile forces exerted by fibroblasts that induce matrix remodeling. Thus, as an initial stage, the optimization of the collagen layer primarily focused on preventing collagen contraction induced by fibroblasts adjusting multiple parameters such as collagen concentration, fibroblast seeding density within the hydrogels, and hydrogel reinforcement with alginate, as detailed in the materials and methods. In previous studies of our team, fibroblasts have been embedded in a collagen layer using a collagen concentration of 6 mg/mL, and a seeding density of  $5 \times 10^4$  cells/mL [39,40]. Initially, these conditions were replicated while testing three different hydrogel volumes per insert (110, 180, and 200  $\mu$ L). Under all tested conditions, fibroblasts contracted the collagen hydrogels (Supplementary Fig. S1). Using a higher collagen concentration (7 mg/mL) under the same HIF seeding density, and hydrogel volumes resulted in less contraction for all volumes tested as demoted by imaging analysis (Supplementary Fig. S1).

**Table 1**

Cytokines and chemokines analyzed using enzyme-linked immunosorbent assay.

Cytokines	Reference	Manufacturer
IL-8	900-M18	PeptoTech
IL-6	900-K16	PeptoTech
IL-10	900-K21	PeptoTech
IL-12	900-T96	PeptoTech
TNF- $\alpha$	900-K25	PeptoTech
CXCL10	900-K39	PeptoTech
CCL20	DY360	R&D

**Table 2**

Cytokines and chemokines composing the Bio-plex Pro array.

Cytokines		Chemokines				
IL-8	IFN- $\gamma$	CCL1	CCL19	CXCL2	CCL25	CXCL12
IL-6	TNF- $\alpha$	CCL2	CCL20	CXCL5	CCL26	CXCL13
Cacl2	GM-CSF	CCL3	CCL21	CXCL6	CCL27	CXCL16
IL-12	MIF	CCL7	CCL22	CXCL9	CXCL1	CX3CL1
IL-1 $\beta$	IL-4	CCL13	CCL23	CXCL10	CCL8	CCL13
IL-2	IL-16	CCL17	CCL24	CXCL11	CCL11	CCL17

Although this concentration seemed optimal to prevent hydrogel contraction, the impact on HIF viability was unknown. The metabolic activity of HIF in both concentrations (6 and 7 mg/mL of collagen) was assessed, as illustrated in Supplementary Fig. S1. Although it is important that fibroblasts do not contract the gel, it is also crucial that they remain healthy and metabolically active within the gels, achieving a compromise between fibroblast proliferation and hydrogel integrity. A notable decrease in metabolic activity was observed in hydrogels with a collagen concentration of 7 mg/mL, compared to the concentration of 6 mg/mL, suggesting that a higher collagen concentration negatively impacted fibroblast metabolic activity (Supplementary Fig. S1). To overcome this, another approach was attempted that included the addition of another polymer, alginate, reinforcing the poor mechanical properties of collagen, while maintaining hydrogel biocompatibility and minimal cytotoxicity [47]. Therefore, collagen concentration was maintained at 6 mg/mL and the HIF density at  $5 \times 10^4$  cells/mL, while different alginate concentrations (2.5, 5, and 10 mg/mL) were tested, across the same hydrogel volumes (Supplementary Fig. S2). Collagen-alginate hydrogels, with a volume of 110  $\mu$ L per insert, exhibited contraction on day 7 after cell seeding. This contraction was prevented at the highest alginate concentration of 10 mg/mL. However, at this concentration, the metabolic activity of HIF decreased notably (Supplementary Fig. S2). Based on the balance between the lowest possible hydrogel volume and better alginate concentration for maintenance of HIF metabolic activity, the condition that showed the most promising outcomes involved the mixture of 2.5 mg/mL alginate with 6 mg/mL of collagen to form the hydrogel, using an optimal volume per insert of 180  $\mu$ L. Based on these results, the alginate concentration was further reduced while varying the cell density. The cell response was reassessed in terms of metabolic activity. We tested the alginate concentration of 1 mg/mL, keeping the concentration of 2.5 mg/mL tested before as a comparison. Also, two HIF densities,  $10^5$  cells/mL (as depicted in Fig. 2A) and  $2 \times 10^5$  cells/mL (Fig. 2B) were tested. The metabolic activity of the HIF was assessed through resazurin assay on days 7, 14, and 21 after embedding.

In both conditions, a significant increase in metabolic activity was observed on day 14, regardless of the hydrogel composition and cell density (Fig. 2), followed by a decrease on day 21. Despite this decrease, fibroblasts remained active throughout the 3-week culture period, indicating their health and proliferation. Notably, the condition with 1 mg/mL alginate concentration and a cell density of  $10^5$  cells/mL exhibited higher levels of metabolic activity compared to the condition with 2.5 mg/mL alginate concentration. This enhancement of fibroblast proliferation and growth at the lower alginate concentration can be attributed to the distinct structural properties of the hydrogels formed at different concentrations. At lower alginate concentrations, such as 1 mg/mL, the hydrogel formed is expected to have a more open and porous structure, allowing better diffusion of nutrients, gases, and growth factors essential for fibroblast viability and proliferation. Additionally, fibroblasts are known for their ability to remodel the extracellular matrix to create an optimal microenvironment for their growth and function. Lower concentrations of alginate may facilitate this remodeling process, promoting cell-matrix interactions and thereby supporting increased proliferation. Overall, the optimal conditions for the lamina propria-like matrix in our 3D IBD model involved a collagen

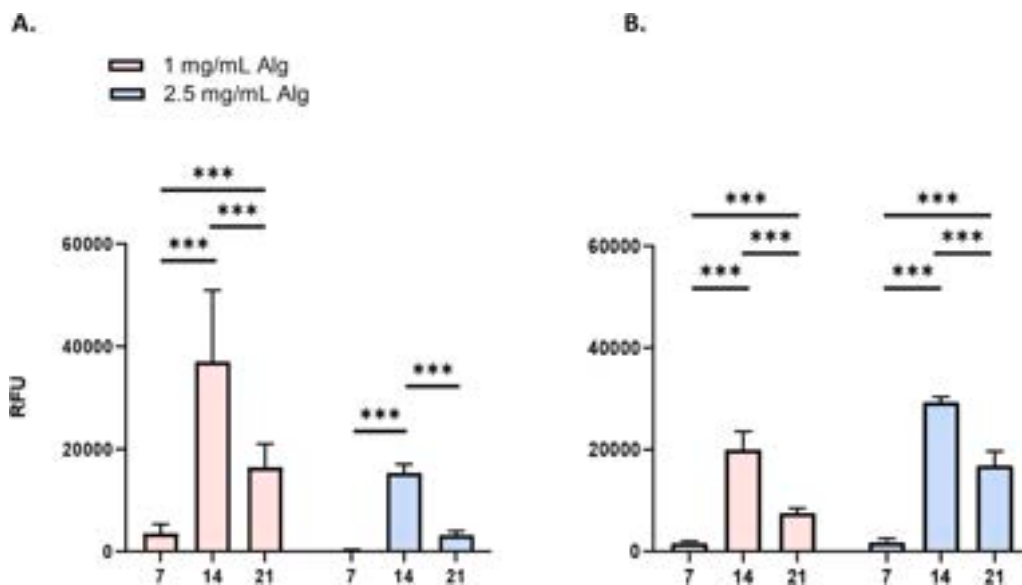


**Fig. 2.** Metabolic activity of HIF at different densities. The metabolic activity of HIF embedded in collagen-alginate hydrogels was evaluated by the resazurin assay at days seven, fourteen, and twenty-one after embedding, at two distinct seeding densities, 10<sup>5</sup> cells/mL (A) and 2 × 10<sup>5</sup> cells/mL (B). Results are presented as mean ± standard deviation (SD) of three independent replicates. Statistical differences at  $p < 0.001$  are denoted by \*\*\*.

concentration of 6 mg/mL, an alginate concentration of 1 mg/mL, and a HIF density of 10<sup>5</sup> cells/mL, providing a balance between structural integrity and cellular activity.

To assess whether the engineered optimal hydrogel matrix was suitable for mimicking the intestinal lamina propria, rheological analyses were conducted to assess their mechanical properties in different conditions (collagen, collagen-alginate, and collagen-alginate with cells). A frequency sweep test was performed (Fig. 3A) within the linear viscoelastic region (0.1–10 Hz, 1 % strain) to determine the Young’s modulus, which reflects the fundamental mechanical properties and stiffness of a material [48]. Within this region, applied stresses do not structurally damage the hydrogels, allowing the determination of mechanical properties such as Young’s modulus. To compare the stiffness ( $\mu$ ) of the different hydrogels, a normalization of the data was performed using the equation  $\mu = \frac{2G'_{\omega}^2}{(G'_{\omega} + G''_{\omega})}$ , in which  $G'$  and  $G''$  correspond to Young’s modulus and the complex modulus, respectively [49]. The average stiffness determined from the frequency sweep at 1 Hz (Fig. 3B) was 328

± 18 Pa and 730 ± 21 Pa for collagen and collagen-alginate hydrogels, respectively. These results demonstrate a significant increase in the stiffness of the hydrogel with the addition of the alginate component. This finding aligns with previous research indicating that adding alginate to collagen hydrogels enhances mechanical properties and is an effective method for tuning hydrogel stiffness [47]. However, the tuning of collagen hydrogel stiffness by adding alginate is dependent on the concentration of Ca<sup>2+</sup> [50], which could explain the mild increase in stiffness. Furthermore, adding cells into the collagen-alginate hydrogel resulted in a slight reduction of the stiffness (126 ± 28 Pa). Some studies suggested that embedded fibroblasts could import Ca<sup>2+</sup> from the alginate cross-linking matrix, increasing its degradation and thus reducing hydrogel stiffness over time. This is particularly important if a lower alginate concentration is used, as the baseline properties of the material are weaker, increasing the risk of gel disintegration *in situ* [51]. Although the average stiffness of the collagen-alginate with cells (126 ± 28 Pa) was not within the typical range of intestinal lamina propria

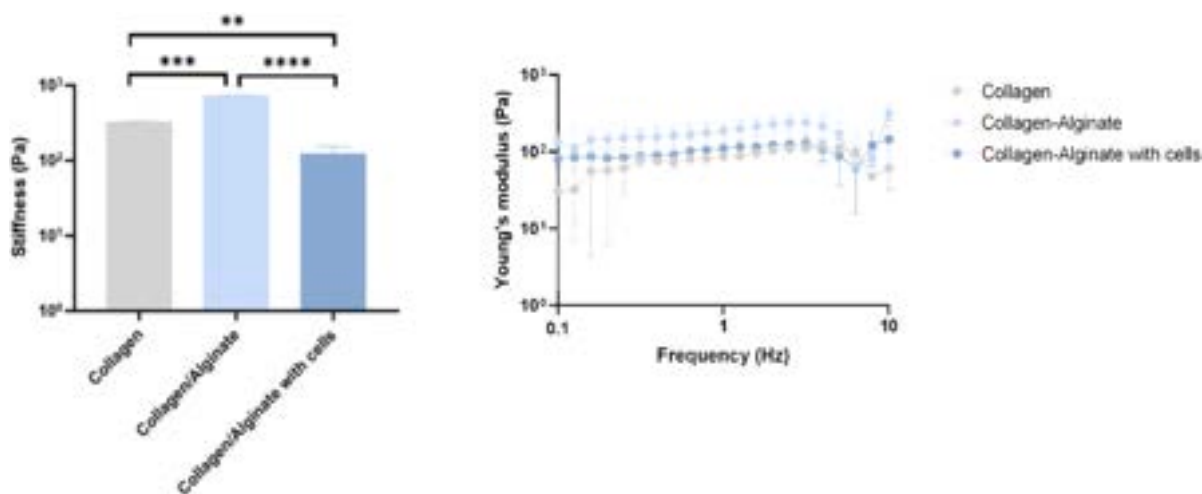


**Fig. 3.** A. Average stiffness determined at 1 Hz within the linear viscoelastic region. B. Rheological behavior and Young’s modulus determination of the different hydrogels when subjected to the frequency sweep test (0.1–10 Hz, 1 % strain). Results are represented as mean ± standard deviation ( $n = 3$ ). Statistical differences were considered significant at \* $p < 0.05$ , \*\* $p < 0.01$ , \*\*\* $p < 0.001$ , \*\*\*\* $p < 0.0001$ .

stiffness (0.5 to 1 kPa) [39], the rheological evaluation confirmed that all hydrogels tested are soft matrices with the potential to modulate stiffness by tuning calcium concentrations. However, the stiffness of the collagen-alginate hydrogel ( $730 \pm 21$  Pa) before cell embedding is aligned with the typical stiffness of the intestinal lamina propria [52,53].

### 3.2. Maintenance of fibroblastic morphology inside the lamina propria-like matrix

To evaluate the HIF morphology in the optimized hydrogel, the collagen-alginate layer was prepared with collagen at a concentration of 6 mg/mL and alginate at 1 mg/mL. The HIF density was set at  $10^5$  cells/mL. HIF were stained with vimentin, a common HIF marker, and f-actin for the cell membrane, and visualized using a high-content screening system equipped with a fully automated widefield/confocal fluorescence microscope (Opera Phenix Screening System). Image analysis revealed fibroblasts in the hydrogel, presenting a prototypical elongated shape (indicated by F-actin staining), and expressing their typical marker (Fig. 4).

### 3.3. Optimization of monocyte-to-macrophage differentiation

Macrophages are known to invade the intestinal mucosa, perpetuating inflammation and tissue damage. For this purpose, a human monocytic cell line, THP-1, was differentiated into macrophages before being added to the herein proposed 3D model. Following PMA exposure, THP-1 cells acquire a macrophage-like phenotype, represented by marked morphological changes such as adherence to culture plates, flat and amoeboid shape, spread morphology, increased cytoplasmic volume and granularity, and irregular nucleus shape, as observed by transmission electron microscopy (Fig. 5B). THP-1 differentiation was further

confirmed through flow cytometry analysis of CD14 expression. THP-1 response to PMA and the resultant levels of CD14 on their surface present conflicting findings in the literature. While it's generally observed that differentiated THP-1 cells exhibit increased cell surface expression of CD14 [54], the extent of this expression varies widely among studies. Some studies reported nearly 90 % CD14 expression in undifferentiated THP-1 cells [55], whereas others indicated lower [56] or even absence of CD14 expression [57]. Similarly, the response of THP-1 CD14 levels to PMA stimulation varies from poor or no response to a marked increase [58,59]. Here, we observed that PMA treatment led to an increased cell-surface expression of CD14 (Fig. 5D) from 16.6 % CD14+ cells without stimulation to 74.3 % when stimulated, as depicted in Fig. 5D.

### 3.4. Integration of the optimized lamina propria-like matrix with embedded HIF and macrophagic population in the 3D intestinal model

Having established the suitable “lamina propria”-like settings and successfully optimizing the differentiation of THP-1 monocytes into macrophages, the 3D IBD model was further developed. This model includes a collagen-alginate-based layer embedded with fibroblasts to mimic the intestinal lamina propria and support the overlying epithelium, which comprises enterocytes and mucus-secreting cells. Macrophages are positioned above the epithelium, while an endothelial layer, simulating the absorptive capillary network, completes the 3D model. Ideally, to mimic the *in vivo* scenario, monocytes should be added to the basolateral compartment, allowing them to migrate and differentiate into macrophages within the intestinal mucosa on the apical side, or pre-differentiated macrophages could be directly added to the intestinal mucosa. However, due to the high sensitivity of macrophages, we anticipated limitations in maintaining their co-culture over 21 days in the 3D model. Consequently, an alternative approach was adopted by introducing PMA-differentiated macrophages at later stages of the 3D

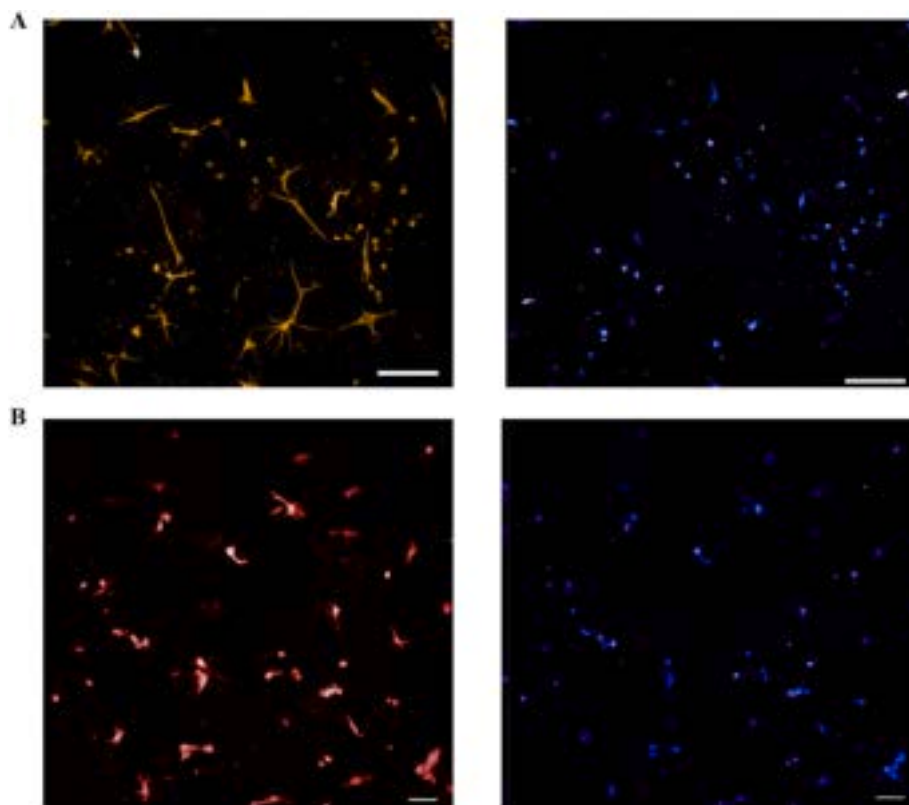


**Fig. 4.** HIF in collagen-alginate hydrogels as observed using the Opera Phenix Plus. A. Immunostaining for vimentin (depicted in yellow). B. Immunostaining for F-actin (displayed in red). Blue represents nuclei. Scale bar in all images is set at 100  $\mu$ m. (For interpretation of the references to colour in this figure legend, the reader is referred to the web version of this article.)

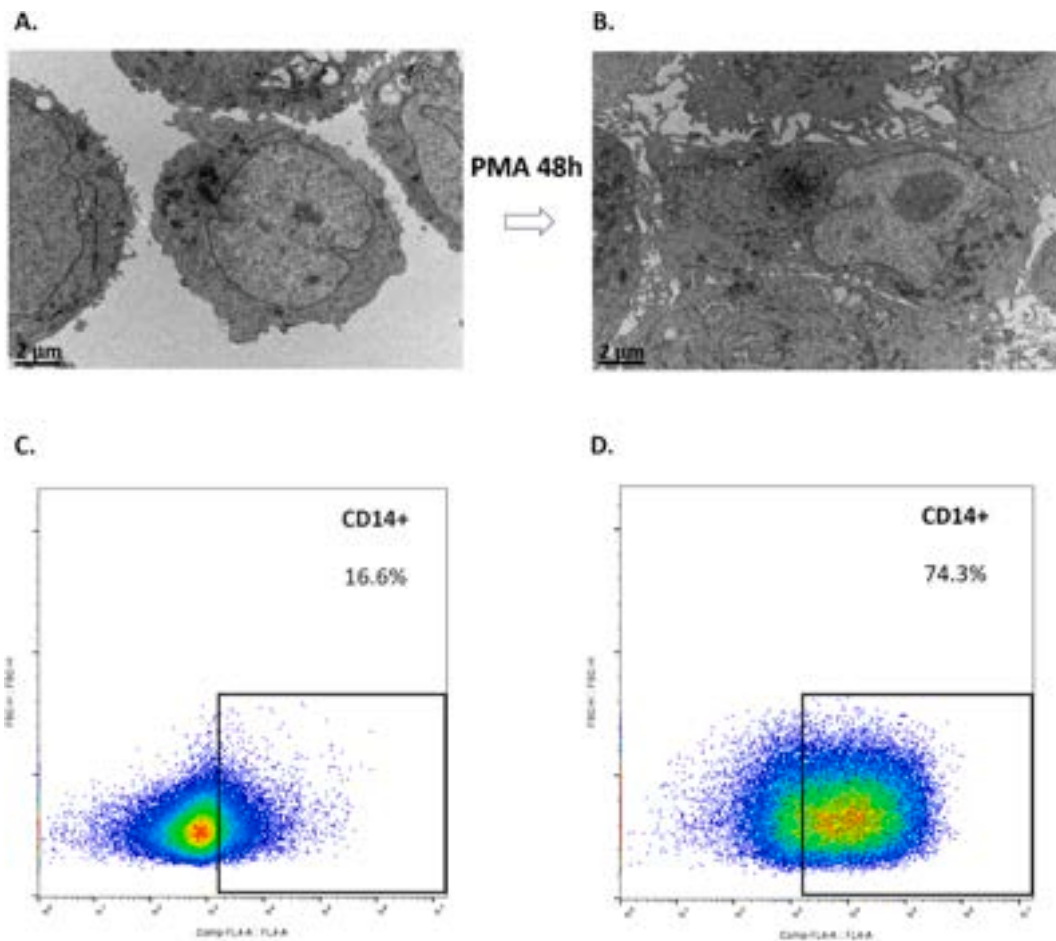


**Fig. 5.** Transmission electron microscopy images of undifferentiated (A) and differentiated (B) THP-1 cells showing morphological changes induced by PMA treatment. Flow cytometry analysis of CD14<sup>+</sup> in undifferentiated (C) and differentiated (D) THP-1 cells.

intestinal model, specifically on the apical side for integration in the epithelial layer.

#### 3.4.1. Cell layer formation and expression of tight junction proteins

Following the addition of macrophages to the apical side of our 3D model, we confirmed the integrity of the epithelial cell layer and the expression of TJs through H&E staining and immunofluorescence. Image analyses demonstrated the integrity of the epithelial layer on top of the hydrogel (Fig. 6A). Additionally, macrophages were observed on the surface of the epithelial layer, as indicated by the arrow in Fig. 6A. On-site immunofluorescence analysis revealed the expression of EpCAM and ZO-1, markers for epithelial cells and tight junctions, respectively. These results corroborate the structural integrity of the epithelial layer after 21 days, as observed with H&E staining (Fig. 6B), even in the presence of macrophages.

### 3.5. Induction of IBD-like state using pro-inflammatory stimuli

#### 3.5.1. Screening of the 3D model response LPS stimulus

A pro-inflammatory triggering compound, namely LPS, was used to mimic the inflammatory microenvironment in the immune-competent intestinal 3D model. LPS at a concentration of 100 ng/mL was added to the apical side of the model and its effects on cytokine production profile was assessed. LPS can trigger a series of immune responses through the activation of various pathways. One of the major pathways is the activation of TLR4. The receptor dimerization leads to the activation of a series of downstream mediators, culminating in the phosphorylation and nuclear translocation of NF- $\kappa$ B and the production of

inflammatory cytokines, including IL-6 and TNF- $\alpha$  [10,60]. The model aimed to mimic intestinal inflammatory processes while causing minimal disruption of the Caco-2 cell monolayer [16]. While some researchers have reported that Caco-2/HT29-MTX co-culture may not respond to LPS treatment (10 ng/mL) [36], others have demonstrated that LPS-induced inflammation in Caco-2 and THP-1 cell lines affected the levels of pro-inflammatory cytokines such as IL-1 $\beta$ , IL-8, IL-6 and TNF- $\alpha$  [61]. Herein, the introduction of macrophages into the 3D intestinal model seemed to contribute to the secretion of pro-inflammatory cytokines, which are crucial markers of inflammation (Fig. 7). Interestingly, the lack of a synergistic effect with LPS suggests that the macrophages alone were sufficient to induce a robust inflammatory response, potentially overshadowing any additional impact of LPS (Fig. 7).

#### 3.5.2. Screening 3D model response to two distinct cytokine cocktail stimuli

Since LPS failed to trigger the robust secretion of pro-inflammatory factors in the 3D immune-competent model, a novel approach using two cytokine cocktails was tested. Cocktail A (TNF- $\alpha$ , IFN- $\gamma$ , and IL-1 $\beta$ ) and Cocktail B (TNF- $\alpha$ , IL-1 $\beta$ , and IL-17 A) at different concentrations of 1 and 10 ng/mL were used. The selection of these cocktails was supported by a thorough review of the literature focusing on well-established signaling pathways and cytokine responses. These selected cytokines are recognized for their ability to activate different signaling pathways implicated in inflammatory responses. TNF- $\alpha$  activates the Nuclear Factor-kappa B (NF- $\kappa$ B) and mitogen-activated protein kinases (MAPKs) signaling pathways, leading to the upregulation of IL-6, IL-8, IL-12, IL-17, IL-1 $\beta$ , and TNF- $\alpha$  [62]. Similarly, IL-17 A also stimulates the

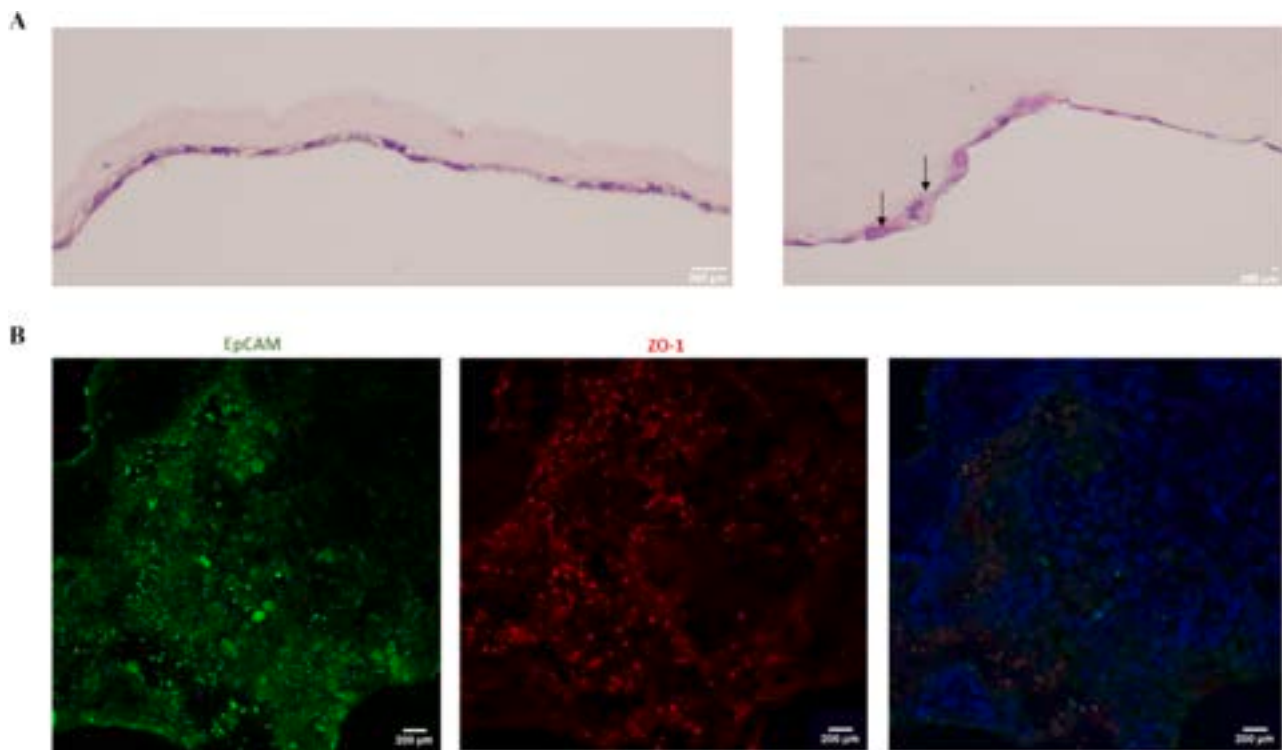


**Fig. 6.** A. H&E staining of the 3D intestinal model at 21 days. B. Immunofluorescence of the co-culture of Caco-2 and HT29-MTX cells on top of the collagen-alginate hydrogels. EpCAM was labeled with Alexa-Fluor 488 (green), and the TJ protein ZO-1 was labeled with Alexa-Fluor 594 (red). The nucleus was counterstained with 4',6-diamidino-2-phenylindole (DAPI) (blue). Scale bar in all images is set at 200  $\mu$ m. (For interpretation of the references to colour in this figure legend, the reader is referred to the web version of this article.)

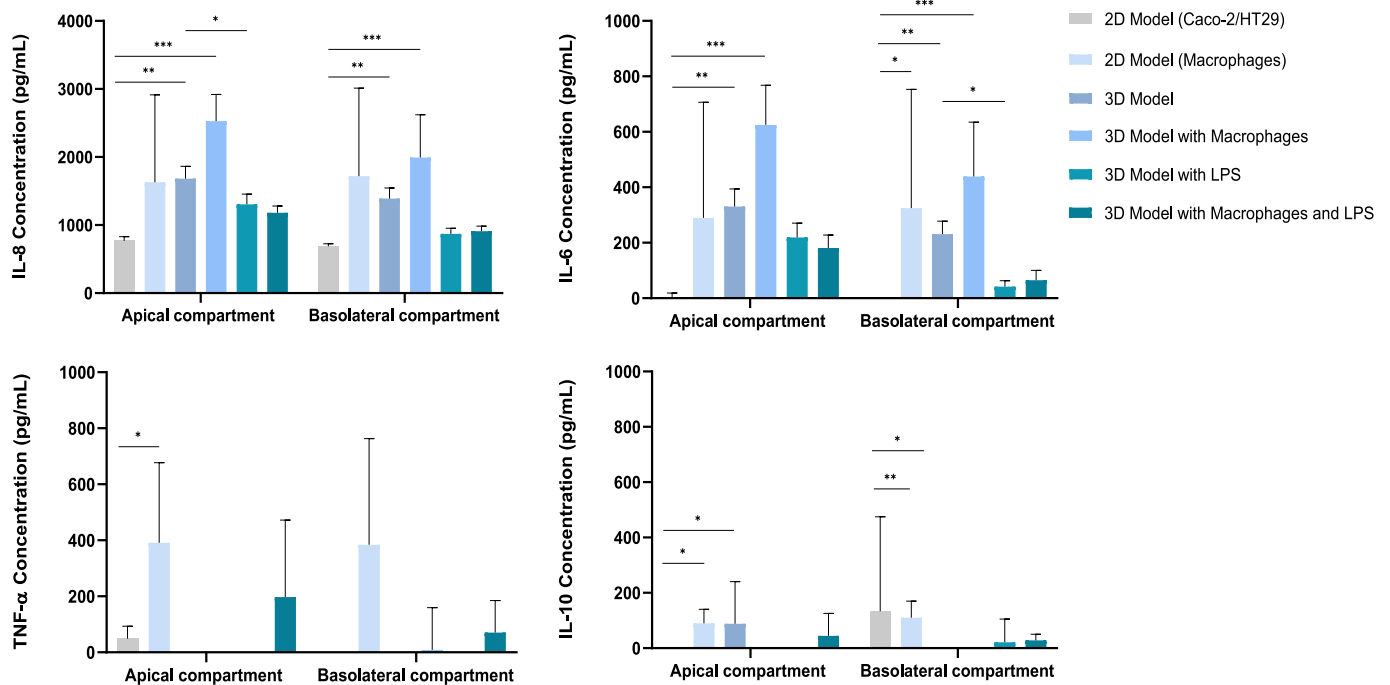


**Fig. 7.** Cytokine production in the 3D intestinal model stimulated with 100 ng/mL concentration of LPS for 24 h. Results are the average of triplicates, and bars represent the standard error of the mean (SEM). Statistical differences at  $p < 0.05$ ,  $p < 0.01$ , and  $p < 0.001$  are denoted by \*, \*\*, and \*\*\*, respectively.

NF- $\kappa$ B and MAPK pathways, contributing to the secretion of additional inflammatory mediators such as IL-22, CXCL1, and GM-CSF. Additionally, IFN- $\gamma$  triggers the JAK-STAT signaling pathway, activating the Janus kinases (JAKs), particularly JAK1 and JAK2, which are

responsible for elevated levels of IL-12, TNF- $\alpha$ , and CXCL10 [63]. Considering these mechanisms, an increased secretion of pro-inflammatory cytokines and chemokines, known to be raised in IBD patients, was anticipated [64]. The cytokine profiles were assayed using

a cytokine array capable of measuring the presence of 40 cytokines and standardized by z-score to highlight relative differences of secreted cytokines between conditions (Fig. 8A). The results indicated notable changes, particularly in CXCL9 and CXCL12 levels, which were more pronounced in the presence of macrophages when using cocktail A after 24 h (Fig. 8A). Although the results from this experiment were not fully elucidative regarding the stimulus induced by each cocktail, we could observe that at 48 h (after half of the medium was replaced by fresh medium, thus removing part of the stimulus) the levels of each analyte were only slightly decreased, suggesting that the levels of cytokine/chemokine were maintained and not reverted (Supplementary Fig. S3). Increased IL-6 levels were observed at 48 h upon cocktail A' stimulation in the presence of macrophages (1.5-fold increase). Similar effects were further observed for IFN- $\gamma$ , suggesting a stronger correlation with the presence of macrophages rather than the cocktail itself (Supplementary Fig. S3). Based on these data, we hypothesized that the early addition of macrophages during the initial phase of the intestinal 3D model development could have impaired the capacity of immune cells to respond to the cocktail (Fig. 8A). To test this hypothesis, we conducted a follow-up experiment where we introduced immune cells on day 19 of the model, 24 h before inducing inflammation. In this second experiment, we observed that cocktail B increased IL-2 production in the 3D model regardless of the presence of macrophages. Notably, this increase was only evident with macrophages at a higher concentration (B') (Fig. 8B). For IL-6 and IL-8, both cocktail A and both concentrations of cocktail B induced cytokine production regardless of macrophage presence. Higher levels of IFN- $\gamma$  seem to be associated with cocktail A and both concentrations of cocktail B, in the presence of macrophages, namely as compared to the 3D model itself. Clearer differences in CCL2 were

noticed in this second experiment, with a pronounced increase in groups with macrophages treated with cocktails A and B' (Fig. 8B). IL-10 levels remained at basal levels, consistent with its primary role in modulating and suppressing inflammatory responses. CCL20 levels were at basal levels, although a mild decrease was observed in some cases. As in the first experiment, CXCL9 levels were higher in the 3D model treated with cocktail A (Fig. 8B). The effects of both cocktails on CXCL10, CXCL11, and CX3CL1 levels were less clear. Overall, these chemokines appeared to be produced regardless of the presence of macrophages. These results suggest that the effects observed were independent of the cocktail concentration, leading us to select the lowest concentration of 1 ng/mL for further experiments. Given the results of both experiments, cocktail A was selected for subsequent studies.

### 3.5.3. Single-cell dynamics in response to cytokine cocktail within the 3D model

To explore the effect of the inflammatory stimuli on the different cell types within this 3D model, individual cells were stimulated with cocktail A for 24 h. This approach was crucial not only to delineate the specific response of each cell type to the pro-inflammatory stimulus but also to evaluate the THP-1 response following differentiation with PMA. The cytokine profiles were assessed focusing on key cytokines/chemokines, including IL-6, IL-8, IL-12, CCL20, and CXCL10. After 24-h exposure to cocktail A, THP-1 cells showed a significant increase in the production of CXCL10 and IL-8 (Fig. 9). This observation aligns with previous studies indicating that IFN- $\gamma$  is a positive regulator of CXCL10 and a negative regulator of IL-8 [65]. Additionally, the combination of IFN- $\gamma$  and TNF- $\alpha$  induced CXCL9/10/11, CCL2/3, and IL-1 $\beta$  secretion in primary human macrophages [65]. However, IL-12 was not highlighted

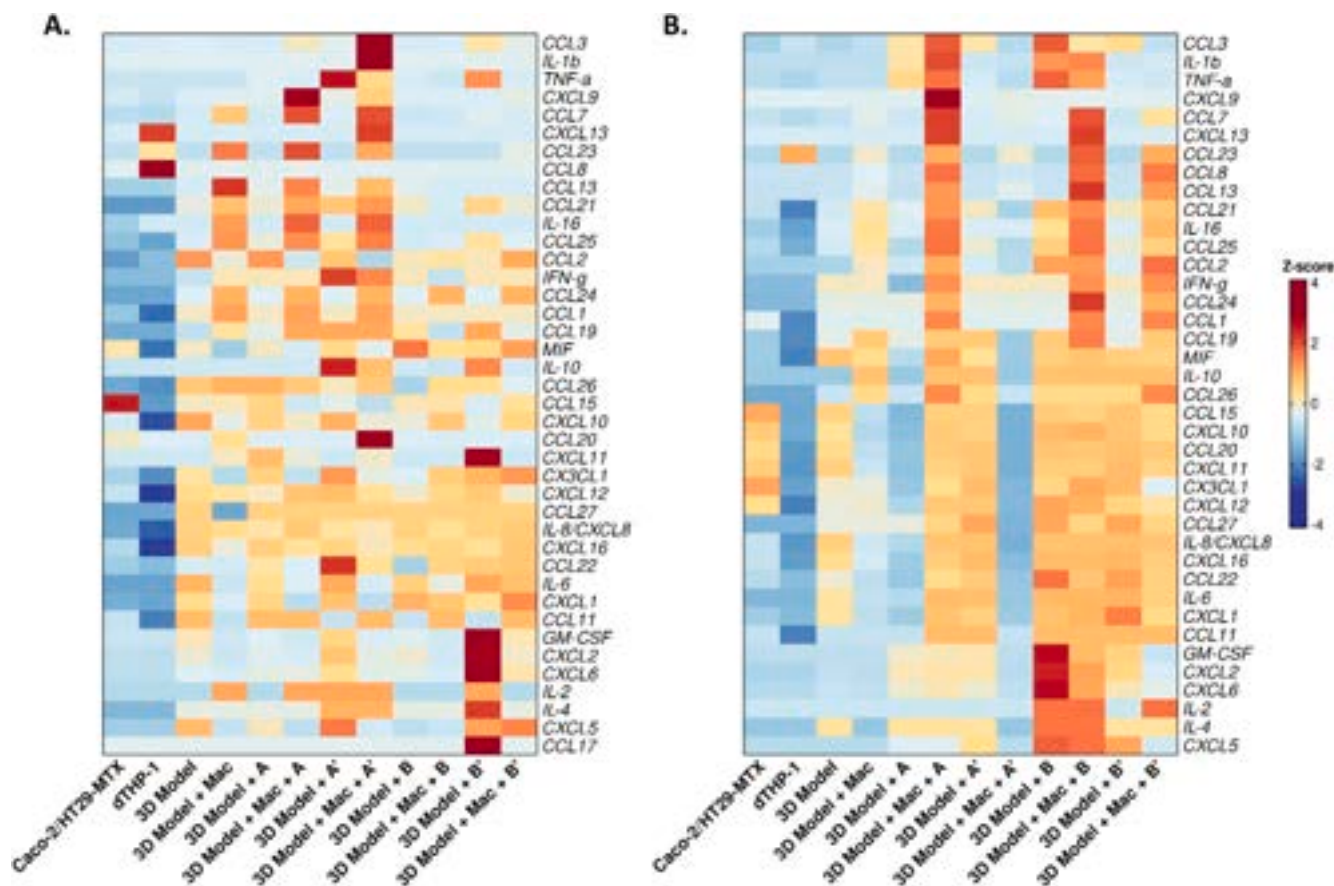
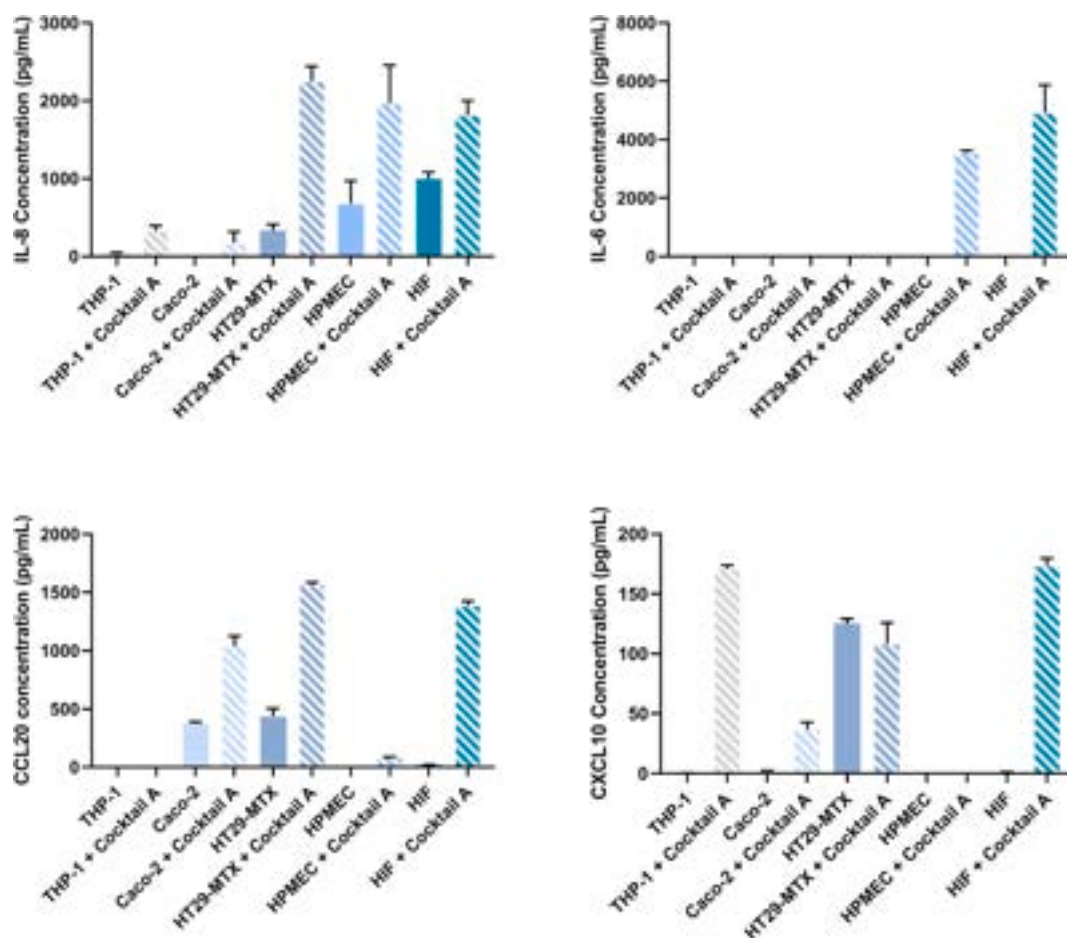


Fig. 8. Multiplex assay for the 3D intestinal inflammatory model with a collagen-alginate lamina propria-like matrix A. Macrophages were added on day 14. B. Macrophages were added on day 19. Heat maps representing cytokine/chemokine panels. Cytokine/chemokine blot intensities were standardized by z-score and reported as heat maps.



**Fig. 9.** Analysis of inflammatory cytokines by ELISA. Comparison of single cells response to cocktail A at 24 h after stimulus. Results are presented as the average of triplicates, and bars represent the standard error of the mean (SEM).

in this work, likely due to its non-detection post-exposure to cocktail A. This result suggests that the combination of TNF- $\alpha$  and IFN- $\gamma$  in cocktail A may not be sufficient to induce IL-12 secretion. This observation is noteworthy, namely considering that THP-1 cells should exclusively produce IL-12. The lack of IL-12 production in THP-1 cells suggests the possibility of including another stimulus in cocktail A to activate pattern recognition receptor (PRR) pathways. Specifically, combining IFN- $\gamma$  with LPS could drive IL-12 production in THP-1 cells, while preserving the effects on other cytokines. In response to cocktail A, HPMEC cells did not produce CXCL10 or CCL20. However, they exhibited increased production of IL-8 and IL-6. Another relevant observation was that HT29-MTX cells showed baseline production levels of CCL20 and CXCL10. The presence of cocktail A did not significantly alter their production levels. Although the cocktail demonstrates effectiveness, it might be beneficial to consider the addition of another stimulus to further enhance the activation of THP-1 cells, specifically regarding the production of IL-12 and IL-6. Upon stimulation, only HPMEC and HIF were capable of producing IL-6, and studies on IL-6 trans-signaling *via* soluble IL-6 receptor complexes have demonstrated that this mechanism stimulates non-immune cells such as fibroblasts, thereby promoting intestinal inflammation and tissue remodeling [66].

Overall, cocktail A triggered a response in all cell types that compose the 3D model.

### 3.5.4. Combined effect of the selected cytokine cocktail and LPS in the 3D model

Finally, to address the potential synergistic effects of combining Cocktail A and LPS, triggering other pathways not activated by TNF- $\alpha$  +

IFN- $\gamma$  + IL-1 $\beta$ , such as the TLR4, a 21-day experiment was conducted. Macrophages were added on day 19 to the 3D intestinal model, and the stimulus was provided on day 20. Culture medium was collected on day 21 and day 25, respectively 24 h and 120 h after the stimulus. Cocktail A appeared to induce a pro-inflammatory microenvironment in the 3D model by increasing the levels of CCL20, IL-6, and CXCL10 (Fig. 10). As anticipated, when combined with LPS, IL-6 levels were significantly elevated as compared to the non-stimulated (N.S.) group. After stimuli removal, the profile of CXCL10 and CCL20 remained consistent over time, up to day 25 (although to a lower extent), In contrast, IL-6 levels reverted to baseline following the removal of stimuli. This observation aligns with other studies, indicating that polarized macrophages often revert to an unpolarized state once external cytokine stimuli are withdrawn [67,68].

## 4. Conclusions

Current *in vitro* disease modeling toolboxes fail to accurately replicate the bioarchitecture of IBD, leading to poorly predicted clinical responses of newly developed therapeutics and the lack of biorelevant platforms for pathophysiology studies. To address these limitations, we proposed a novel and robust 3D *in vitro* model of IBD consisting of a multi-layered Transwell® system featuring an immune component and mimicking inflammatory conditions. This 3D model features a collagen-alginate matrix embedded with fibroblasts to mimic the intestinal lamina propria, supporting an overlying epithelium composed of enterocytes and mucus-secreting cells. Macrophages are located above the epithelium, and an endothelial layer simulating the absorptive capillary

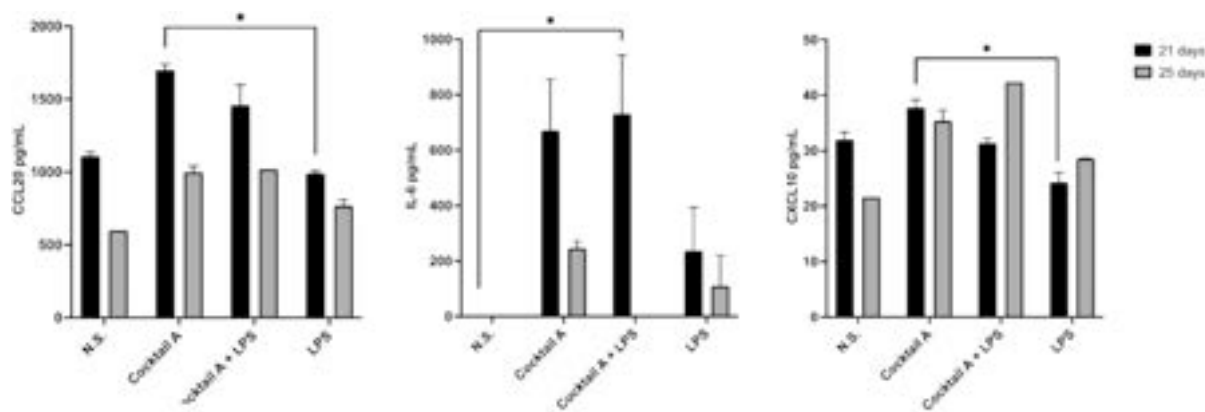


**Fig. 10.** ELISA analysis of the 3D model response to the combined effects of Cocktail A and LPS. Results are presented as mean  $\pm$  standard deviation (SD) of three independent replicates. Statistical differences at  $p < 0.01$  are denoted by \*.

network completes the 3D model. The lamina propria-like matrix of rat tail collagen type I was mechanically reinforced with alginate to avoid fibroblast-induced matrix contraction over time. The collagen-alginate composite hydrogel provided optimal conditions for the maintenance of HIF metabolic activity and morphology over time. Pre-differentiated THP-1-derived macrophages were added on day 19 to confer the developed 3D model with specific immune response capability. A pro-inflammatory microenvironment was induced by adding a specialized inflammatory cocktail, optimized in terms of composition, concentration, and incubation time. The ideal combination consisted of TNF- $\alpha$ , IFN- $\gamma$ , and IL-1 $\beta$  (1 ng/mL each) along with LPS (100 ng/mL), added to the model on day 20 for 24 h. Although initial attempts to induce an inflammatory response using LPS alone were insufficient, the 3D model responded robustly to the cytokine cocktail, especially when macrophages were introduced later in the experimental timeline. This pro-inflammatory stimulus effectively triggered the secretion of pro-inflammatory cytokines and chemokines, including CCL20, IL-6, CXCL9, and CXCL10, which are key markers of IBD. This 3D model stands out for its ability to replicate essential aspects of intestinal inflammation and provides a versatile platform for screening potential therapeutic candidates for IBD. At the forefront of high-throughput drug discovery and personalized medicine, this innovative platform offers valuable insights into the mechanisms underlying intestinal repair by elucidating the responses of epithelial, mesenchymal, immune, and endothelial cells to inflammatory stimuli. Beyond its application to IBD, this approach holds potential to be adapted for developing 3D *in vitro* models of other inflammatory processes across a range of tissues and organs.

## Funding

Funded by the European Union (GA 101057491) and supported by the UK's innovation agency, Innovate UK and the Swiss State Secretariat for Education, Research and Innovation (SERI) under contract number 22.00119. Views and opinions expressed are however those of the author(s) only and do not necessarily reflect those of the European Union or the European Health and Digital Executive Agency (HADEA). Neither the European Union nor the granting authority can be held responsible for them.

## CRedit authorship contribution statement

**Bárbara Ferreira:** Writing – original draft, Methodology, Formal analysis, Data curation. **Cecília Ferreira:** Writing – original draft, Methodology, Investigation. **Cláudia Martins:** Writing – original draft, Methodology, Data curation. **Rute Nunes:** Writing – review & editing, Validation, Investigation, Conceptualization. **José das Neves:** Writing –

review & editing, Validation. **Catarina Leite-Pereira:** Writing – review & editing, Supervision, Methodology, Data curation. **Bruno Sarmento:** Writing – review & editing, Supervision, Funding acquisition, Conceptualization.

## Declaration of competing interest

The authors declare no conflict of interest.

## Data availability

The data that support the findings of this study are available from the corresponding author upon reasonable request.

## Acknowledgments

This work was supported by the European Commission, proposal 101057491, GENEGUT. of HORIZON-HLTH-2021-TOOL. BF and J.d.N. gratefully acknowledge Fundação para a Ciência e a Tecnologia, Portugal, for their financial support through PhD grant (2024.03050. BD), Individual CEEC Program (CEECIND/01280/2018), respectively. RN acknowledges the support of the Litwin IBD Pioneers initiative Project 937924, formerly known as the Broad Medical Research Program at the Crohn's & Colitis Foundation. The authors acknowledge the support of the i3S Scientific Platforms Bioimaging and Histology and Electron Microscopy (HEMS), members of the national infrastructure PPBI Portuguese Platform of Bioimaging (PPBI-POCI-01-0145-FEDER-022122). The authors also acknowledge the support of the Biochemical and Biophysical Technologies, Biointerfaces and Nanotechnology, and Translational Cytometry i3S Scientific Platforms.

## Appendix A. Supplementary data

Supplementary data to this article can be found online at <https://doi.org/10.1016/j.jconrel.2024.11.070>.

## References

- [1] R.B. Sartor, S.K. Mazmanian, Intestinal microbes in inflammatory bowel diseases, *Am. J. Gastroenterol. Suppl.* 1 (2012) 15.
- [2] M.E. Araruna, C. Serafim, E. Alves Júnior, C. Hiruma-Lima, M. Diniz, L. Batista, Intestinal anti-inflammatory activity of terpenes in experimental models (2010–2020): a review, *Molecules* 25 (2020) 5430.
- [3] S.C. Ng, H.Y. Shi, N. Hamidi, F.E. Underwood, W. Tang, E.I. Benchimol, R. Panaccione, S. Ghosh, J.C.Y. Wu, F.K.L. Chan, J.J.Y. Sung, G.G. Kaplan, Worldwide incidence and prevalence of inflammatory bowel disease in the 21st century: a systematic review of population-based studies, *Lancet* 390 (2017) 2769–2778.
- [4] K.L. Glassner, B.P. Abraham, E.M.M. Quigley, The microbiome and inflammatory bowel disease, *J. Allergy Clin. Immunol.* 145 (2020) 16–27.

- [5] K. Matsuoka, T. Kanai, The gut microbiota and inflammatory bowel disease, *Semin. Immunopathol.* 37 (2015) 47–55.
- [6] N.A. Hering, J.D. Schulzke, Therapeutic options to modulate barrier defects in inflammatory bowel disease, *Dig. Dis.* 27 (2009) 450–454.
- [7] G.P. Ramos, K.A. Papadakis, Mechanisms of disease: inflammatory bowel diseases, *Mayo Clin. Proc.* 94 (2019) 155–165.
- [8] O. Hartwig, M.A. Shetab Boushehri, K.S. Shalaby, B. Loretz, A. Lamprecht, C.-M. Lehr, Drug delivery to the inflamed intestinal mucosa – targeting technologies and human cell culture models for better therapies of IBD, *Adv. Drug Deliv. Rev.* 175 (2021) 113828.
- [9] F.A.R. Silva, B.L. Rodrigues, M.D.L.S. Ayrizono, R.F. Leal, The immunological basis of inflammatory bowel disease, *Gastroenterol. Res. Pract.* 2016 (2016), 2097274–2097274.
- [10] Y.C. Lu, W.C. Yeh, P.S. Ohashi, LPS/TLR4 signal transduction pathway, *Cytokine* 42 (2008) 145–151.
- [11] F. Borcherding, M. Nitschke, G. Hundorfean, J. Rupp, D. von Smolinski, K. Bieber, C. van Kooten, H. Lehnert, K. Fellermann, J. Büning, The CD40-CD40L pathway contributes to the proinflammatory function of intestinal epithelial cells in inflammatory bowel disease, *Am. J. Pathol.* 176 (2010) 1816–1827.
- [12] Q. Li, Q. Zhang, M. Wang, S. Zhao, J. Ma, N. Luo, N. Li, Y. Li, G. Xu, J. Li, Interferon- $\gamma$  and tumor necrosis factor- $\alpha$  disrupt epithelial barrier function by altering lipid composition in membrane microdomains of tight junction, *Clin. Immunol.* 126 (2008) 67–80.
- [13] A. Shahini, A. Shahini, Role of interleukin-6-mediated inflammation in the pathogenesis of inflammatory bowel disease: focus on the available therapeutic approaches and gut microbiome, *J. Cell Commun. Sig.* 17 (2023) 55–74.
- [14] R. Al-Sadi, M. Boivin, T. Ma, Mechanism of cytokine modulation of epithelial tight junction barrier, *Front. Biosci.-Landmark* 14 (2009) 2765–2778.
- [15] I. Comerford, M. Bunting, K. Fenix, S. Haylock-Jacobs, W. Litchfield, Y. Harata-Lee, M. Turvey, J. Brazzatti, C. Gregor, P. Nguyen, E. Kara, S.R. McColl, An immune paradox: how can the same chemokine axis regulate both immune tolerance and activation? CCR6/CCL20: a chemokine axis balancing immunological tolerance and inflammation in autoimmune disease, *Bioessays* 32 (2010) 1067–1076.
- [16] A.A.M. Kämpfer, P. Urbán, S. Gioria, N. Kanase, V. Stone, A. Kinsner-Ovaskainen, Development of an in vitro co-culture model to mimic the human intestine in healthy and diseased state, *Toxicol. In Vitro* 45 (2017) 31–43.
- [17] F. Leonard, E.M. Collnot, C.M. Lehr, A three-dimensional coculture of enterocytes, monocytes and dendritic cells to model inflamed intestinal mucosa in vitro, *Mol. Pharm.* 7 (2010) 2103–2119.
- [18] M. Belaid, J. Javorovic, G. Pastorin, D. Vllasaliu, Development of an in vitro co-culture model using Caco-2 and J774A.1 cells to mimic intestinal inflammation, *Eur. J. Pharm. Biopharm.* 197 (2024) 114243.
- [19] M.L. Coluccio, G. Perozziello, N. Malara, E. Parrotta, P. Zhang, F. Gentile, T. Limongi, P.M. Raj, G. Cuda, P. Candeloro, E. Di Fabrizio, Microfluidic platforms for cell cultures and investigations, *Microelectron. Eng.* 208 (2019) 14–28.
- [20] N.J. Darling, C.L. Mobbs, A.L. González-Hau, M. Freer, S. Przyborski, Bioengineering novel in vitro co-culture models that represent the human intestinal mucosa with improved Caco-2 structure and barrier function, *Front. Bioeng. Biotechnol.* 8 (2020) 992.
- [21] J. Susewind, C. de Souza Carvalho-Wodarz, U. Repnik, E.M. Collnot, N. Schneider-Daum, G.W. Griffiths, C.M. Lehr, A 3D co-culture of three human cell lines to model the inflamed intestinal mucosa for safety testing of nanomaterials, *Nanotoxicology* 10 (2016) 53–62.
- [22] F. Araújo, C. Pereira, J. Costa, C. Barrias, P.L. Granja, B. Sarmiento, In vitro M-like cells genesis through a tissue-engineered triple-culture intestinal model, *J. Biomed. Mater. Res. B Appl. Biomater.* 104 (2016) 782–788.
- [23] A. des Rieux, V. Fievez, I. Theate, J. Mast, V. Preat, Y.J. Schneider, An improved in vitro model of human intestinal follicle-associated epithelium to study nanoparticle transport by M cells, *Eur. J. Pharm. Sci.* 30 (2007) 380–391.
- [24] A. Mori, H. Satsu, M. Shimizu, New model for studying the migration of immune cells into intestinal epithelial cell monolayers, *Cytotechnology* 43 (2003) 57–64.
- [25] T. Tanoue, Y. Nishitani, K. Kanazawa, T. Hashimoto, M. Mizuno, In vitro model to estimate gut inflammation using co-cultured Caco-2 and RAW264.7 cells, *Biochem. Biophys. Res. Commun.* 374 (2008) 565–569.
- [26] M. Galvez-Llompert, M. Del Carmen Recio, J. Iglesias, R. García-Domenech Gálvez, Novel potential agents for ulcerative colitis by molecular topology: suppression of IL-6 production in Caco-2 and RAW 264.7 cell lines, *Mol. Divers.* 17 (2013) 573–593.
- [27] N. Makon-Sébastien, F. Francis, S. Eric, V.P. Henri, L.J. François, P. Laurent, B. Yves, C. Serge, Lycopene modulates THP1 and Caco2 cells inflammatory state through transcriptional and nontranscriptional processes, *Mediat. Inflamm.* 2014 (2014) 507272.
- [28] A. Kaulmann, S. Legay, Y.J. Schneider, L. Hoffmann, T. Bohn, Inflammation related responses of intestinal cells to plum and cabbage digesta with differential carotenoid and polyphenol profiles following simulated gastrointestinal digestion, *Mol. Nutr. Food Res.* 60 (2016) 992–1005.
- [29] J.Y. Kasper, M.I. Hermanns, C. Cavalius, A. Kraegeloh, T. Jung, R. Danzebrink, R. E. Unger, C.J. Kirkpatrick, The role of the intestinal microvasculature in inflammatory bowel disease: studies with a modified Caco-2 model including endothelial cells resembling the intestinal barrier in vitro, *Int. J. Nanomedicine* 11 (2016) 6353–6364.
- [30] P. Worthington, K.M. Drake, Z. Li, A.D. Napper, D.J. Pochan, S.A. Langhans, Implementation of a high-throughput pilot screen in peptide hydrogel-based three-dimensional cell cultures, *SLAS Discov.* 24 (2019) 714–723.
- [31] S.A. Langhans, Three-dimensional in vitro cell culture models in drug discovery and drug repositioning, *Front. Pharmacol.* 9 (2018).
- [32] N. Li, D. Wang, Z. Sui, X. Qi, L. Ji, X. Wang, L. Yang, Development of an improved three-dimensional in vitro intestinal mucosa model for drug absorption evaluation, *Tissue Eng. Part C: Methods* 19 (2013) 708–719.
- [33] M. Ravi, V. Parameash, S.R. Kaviya, E. Anuradha, F.D.P. Solomon, 3D cell culture systems: advantages and applications, *J. Cell. Physiol.* 230 (2015) 16–26.
- [34] Z. Yuan, K. Memarzadeh, A.S. Stephen, R.P. Allaker, R.A. Brown, J. Huang, Development of a 3D collagen model for the in vitro evaluation of magnetic-assisted osteogenesis, *Sci. Rep.* 8 (2018) 16270.
- [35] S. Hinderer, S.L. Layland, K. Schenke-Layland, ECM and ECM-like materials — biomaterials for applications in regenerative medicine and cancer therapy, *Adv. Drug Deliv. Rev.* 97 (2016) 260–269.
- [36] D. Marescotti, G. Lo Sasso, D. Guerrero, K. Renggli, P.A. Ruiz Castro, R. Pialut, V. Jaquet, F. Moine, K. Luettich, S. Frentzel, M.C. Peitsch, J. Hoeng, Development of an advanced multicellular intestinal model for assessing immunomodulatory properties of anti-inflammatory compounds, *Front. Pharmacol.* 12 (2021).
- [37] C. Beaurivage, A. Kanapekaite, C. Loomans, K.S. Erdmann, J. Stallen, R.A. Janssen, Development of a human primary gut-on-a-chip to model inflammatory processes, *Sci. Rep.* 10 (2020) 21475.
- [38] O.T.P. Nguyen, P.M. Misun, A. Hierlemann, C. Lohasz, A versatile intestine-on-chip system for deciphering the immunopathogenesis of inflammatory bowel disease, *Adv. Healthc. Mater.* 13 (2024) e2302454.
- [39] M.H. Macedo, E. Martinez, C. Barrias, B. Sarmiento, Development of an improved 3D in vitro intestinal model to perform permeability studies of paracellular compounds, *Front. Bioeng. Biotechnol.* 8 (2020).
- [40] M.H. Macedo, A.S. Barros, E. Martínez, C.C. Barrias, B. Sarmiento, All layers matter: innovative three-dimensional epithelium-stroma-endothelium intestinal model for reliable permeability outcomes, *J. Control. Release* 341 (2022) 414–430.
- [41] T.D. Allen, S.L. Schor, The contraction of collagen matrices by dermal fibroblasts, *J. Ultrastruct. Res.* 83 (1983) 205–219.
- [42] Y.K. Zhu, T. Umino, X.D. Liu, H.J. Wang, D.J. Romberger, J.R. Spurzem, S. I. Rennard, Contraction of fibroblast-containing collagen gels: initial collagen concentration regulates the degree of contraction and cell survival, *In Vitro Cell. Dev. Biol. Anim.* 37 (2001) 10–16.
- [43] T. Zhang, J.H. Day, X. Su, A.G. Guadarrama, N.K. Sandbo, S. Esnault, L. C. Denlinger, E. Berthier, A.B. Theberge, Investigating fibroblast-induced collagen gel contraction using a dynamic microscale platform, *Front. Bioeng. Biotechnol.* 7 (2019) 196.
- [44] J.P. Bras, A.M. Silva, G.A. Calin, M.A. Barbosa, S.G. Santos, M.I. Almeida, miR-195 inhibits macrophages pro-inflammatory profile and impacts the crosstalk with smooth muscle cells, *PLoS One* 12 (2017) e0188530.
- [45] N. Li, R.H. Shi, Updated review on immune factors in pathogenesis of Crohn's disease, *World J. Gastroenterol.* 24 (2018) 15–22.
- [46] M.F. Neurath, Cytokines in inflammatory bowel disease, *Nat. Rev. Immunol.* 14 (2014) 329–342.
- [47] T. Hu, A.C.Y. Lo, Collagen-alginate composite hydrogel: application in tissue engineering and biomedical sciences, *Polymers (Basel)* 13 (2021).
- [48] A. Guo, B. Wang, C. Lyu, W. Li, Y. Wu, L. Zhu, R. Bi, C. Huang, J.J. Li, Y. Du, Consistent apparent Young's modulus of human embryonic stem cells and derived cell types stabilized by substrate stiffness regulation promotes lineage specificity maintenance, *Cell Regen* 9 (2020) 15.
- [49] Z. Yin, A.J. Romano, A. Manduca, R.L. Ehman, J. Huston 3rd, Stiffness and beyond: what MR Elastography can tell us about brain structure and function under physiologic and pathologic conditions, *Top. Magn. Reson. Imaging* 27 (2018) 305–318.
- [50] F. Charbonier, D. Indana, O. Chaudhuri, Tuning viscoelasticity in alginate hydrogels for 3D cell culture studies, *Curr. Protoc.* 1 (2021) e124.
- [51] N.C. Hunt, A.M. Smith, U. Gbureck, R.M. Shelton, L.M. Grover, Encapsulation of fibroblasts causes accelerated alginate hydrogel degradation, *Acta Biomater.* 6 (2010) 3649–3656.
- [52] J. Costa, A. Ahluwalia, Advances and current challenges in intestinal in vitro model engineering: a digest, *Front. Bioeng. Biotechnol.* 7 (2019) 144.
- [53] D.C. Stewart, D. Berrie, J. Li, X. Liu, C. Rickerson, D. Mkoji, A. Iqbal, S. Tan, A. L. Doty, S.C. Glover, C.S. Simmons, Quantitative assessment of intestinal stiffness and associations with fibrosis in human inflammatory bowel disease, *PLoS One* 13 (2018) e0200377.
- [54] P.B. Aldo, V. Craveiro, S. Guller, G. Mor, Effect of culture conditions on the phenotype of THP-1 monocyte cell line, *Am. J. Reprod. Immunol.* 70 (2013) 80–86.
- [55] N. Foster, J. Cheetham, J.J. Taylor, P.M. Preshaw, VIP inhibits *Porphyromonas gingivalis* LPS-induced immune responses in human monocytes, *J. Dent. Res.* 84 (2005) 999–1004.
- [56] H. Bosshart, M. Heinzmann, THP-1 cells as a model for human monocytes, *Ann. Transl. Med.* 4 (2016) 438.
- [57] P.S. Tobias, K. Soldau, L. Kline, J.D. Lee, K. Kato, T.P. Martin, R.J. Ulevitch, Cross-linking of lipopolysaccharide (LPS) to CD14 on THP-1 cells mediated by LPS-binding protein, *J. Immunol.* 150 (1993) 3011–3021.
- [58] E.K. Park, H.S. Jung, H.I. Yang, M.C. Yoo, C. Kim, K.S. Kim, Optimized THP-1 differentiation is required for the detection of responses to weak stimuli, *Inflamm. Res.* 56 (2007) 45–50.
- [59] J. Ding, L. Lin, W. Hang, X. Yan, Beryllium uptake and related biological effects studied in THP-1 differentiated macrophages, *Metallomics* 1 (2009) 471–478.
- [60] M. Stephens, P.Y. von der Weid, Lipopolysaccharides modulate intestinal epithelial permeability and inflammation in a species-specific manner, *Gut Microbes* 11 (2020) 421–432.
- [61] N. Yahfoufi, N. Alsadi, M. Jambi, C. Matar, The immunomodulatory and anti-inflammatory role of polyphenols, *Nutrients* 10 (2018).

- [62] J.H. Shi, S.C. Sun, Tumor necrosis factor receptor-associated factor regulation of nuclear factor  $\kappa$ B and mitogen-activated protein kinase pathways, *Front. Immunol.* 9 (2018) 1849.
- [63] X. Hu, J. Li, M. Fu, X. Zhao, W. Wang, The JAK/STAT signaling pathway: from bench to clinic, signal transduction and targeted, *Therapy* 6 (2021) 402.
- [64] L. Monin, S.L. Gaffen, Interleukin 17 family cytokines: signaling mechanisms, biological activities, and therapeutic implications, *Cold Spring Harb. Perspect. Biol.* 10 (2018).
- [65] F. Zhang, J.R. Mears, L. Shakib, J.I. Beynor, S. Shanaj, I. Korsunsky, A. Nathan, L. T. Donlin, S. Raychaudhuri, IFN- $\gamma$  and TNF- $\alpha$  drive a CXCL10+ CCL2+ macrophage phenotype expanded in severe COVID-19 lungs and inflammatory diseases with tissue inflammation, *Genome Med.* 13 (2021) 64.
- [66] M.F. Neurath, Strategies for targeting cytokines in inflammatory bowel disease, *Nat. Rev. Immunol.* 24 (2024) 559–576.
- [67] S.X. Liu, H.H. Gustafson, D.L. Jackson, S.H. Pun, C. Trapnell, Trajectory analysis quantifies transcriptional plasticity during macrophage polarization, *Sci. Rep.* 10 (2020) 12273.
- [68] R.D. Stout, J. Suttles, Functional plasticity of macrophages: reversible adaptation to changing microenvironments, *J. Leukoc. Biol.* 76 (2004) 509–513.